SISSA

Low Gain Avalanche Detectors (LGAD) for particle physics and synchrotron applications

To cite this article: N. Moffat *et al* 2018 *JINST* **13** C03014

View the article online for updates and enhancements.

Recent citations

Low Gain Avalanche Detectors (LGAD) for particle physics and synchrotron applications

N. Moffat,[a,1] R. Bates,[a] M. Bullough,[b] L. Flores,[a] D. Maneuski,[a] L. Simon,[a] N. Tartoni,[c]
F. Doherty[a] and J. Ashby[a]

[a]*SUPA School of Physics and Astronomy, University of Glasgow,*
University Avenue, Glasgow, Scotland, U.K.

[b]*Micron Semiconductor Ltd,*
Sussex, U.K.

[c]*Diamond Light Source,*
Oxfordshire, U.K.

E-mail: n.moffat.1@research.gla.ac.uk

Abstract: A new avalanche silicon detector concept is introduced with a low gain in the region of ten, known as a Low Gain Avalanche Detector, LGAD. The detector's characteristics are simulated via a full process simulation to obtain the required doping profiles which demonstrate the desired operational characteristics of high breakdown voltage (500 V) and a gain of 10 at 200 V reverse bias for X-ray detection. The first low gain avalanche detectors fabricated by Micron Semiconductor Ltd are presented. The doping profiles of the multiplication junctions were measured with SIMS and reproduced by simulating the full fabrication process which enabled further development of the manufacturing process. The detectors are 300 μm thick p-type silicon with a resistivity of 8.5 kΩcm, which fully depletes at 116 V. The current characteristics are presented and demonstrate breakdown voltages in excess of 500 V and a current density of 40 to 100 nAcm^{-2} before breakdown measured at 20°C. The gain of the LGAD has been measured with a red laser (660 nm) and shown to be between 9 and 12 for an external bias voltage range from 150 V to 300 V.

---

[1]Corresponding author.

2018 JINST 13 C03014

Contents

1   Introduction

Silicon radiation detectors, based on the PIN diode, are well established in high energy physics experiments [1]. The PIN diode, operated with an external reverse bias in full depletion, produces a signal proportional to the energy deposited by the incident radiation. In addition to particle physics, silicon photodetectors have more recently been widely used at synchrotron sources as x-ray detectors [2]. Silicon detectors are used due to their outstanding features [3], including, their compact size, high quantum efficiency for a wide wavelength range, and high spatial resolution defined by the diode segmentation as either pad, strip or pixels. In order to detect low energy particles and low energy x-rays the Avalanche Photodiode (APD) was developed, this type of detector exhibits an internal signal gain, proportional to the applied bias voltage, with good uniformity across large detection areas [4]. Operation of such a device in the linear region provides a signal output proportional to the absorbed energy, with a gain factor between 10–100, allowing detection of low intensity signals of a few photons. However, there is noise associated with the multiplication process which can distort the signal-to-noise ratio, moreover the leakage current levels associated with APDs are far too high to be compatible with modern readout electronics used in particle physics and hybrid pixel detectors.

The modification of the doping levels in the APD enables the production of a device with a lower gain, in the region of 5–10, which is operated in the linear mode for a proportional response. Such devices are known as Low Gain Avalanche Detectors (LGAD). They are operated at a low voltage and therefore require a high resistivity silicon substrate (5–10 kΩcm) to achieve full depletion. The lower gain reduces noise and detector gain dependence on device temperature and applied bias voltage compared to standard APDs.

The diode can be segmented in the same fashion as standard PIN detectors as the low gain avoids cross-talk. Hybrid pixel detectors can therefore be fabricated that enable the detection of low energy x-rays which produce signals below the noise floor of the electronics. For example, a silicon detector coupled to the Medipix chip [5] has a minimum detectable signal of ≈ 1000 electrons, to be above the noise floor, which corresponds to an incident x-ray of ≈ 4keV. An LGAD device coupled to the Medipix chip with a gain of 10 would enable detection of a 400 eV energy x-ray.

The LGAD design enables the detection of sub-ns signals produced by minimum ionising particles, where the ionisation is produced uniformly as a function of depth in the detector. For an LGAD with a gain of 10, if the LGAD substrate is thinned by an order of magnitude compared to a standard PIN silicon detector the same signal will be produced from a minimum ionising particle by the two devices. The collection time will however be increased by an order of magnitude. The LGAD structure produces a fast rise time and fast silicon timing detectors with sub-ns rise times are therefore possible.

2 LGAD concept

The basic doping profiles of the LGAD structure, based on a standard PIN detector, is shown in figure 1, showing a $n^+/p/p^-/p^+$ structure.
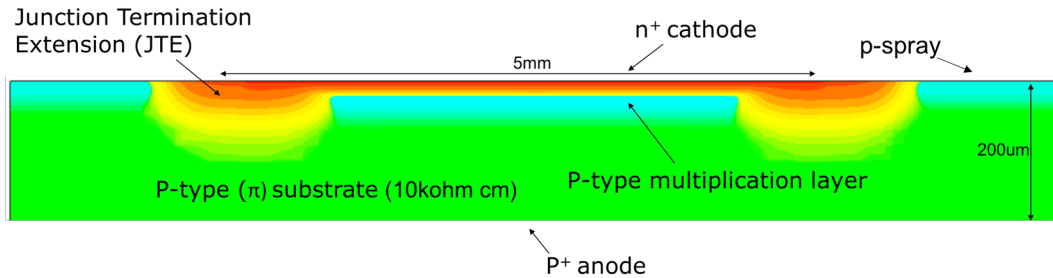

Figure 1. Schematic cross-section of the LGAD pad design. A p-type layer is diffused below the N$^+$ electrode to form the $n^+/p/p^-$ junction where the multiplication takes place.

The figure shows a highly doped n^+ cathode electrode with a moderately doped p-type region below, known as the multiplication implant. The n-type electrode has a peak doping concentration of order 1×10^{19} cm^{-3} and has a shallow profile into the bulk of $\approx 1\,\mu$m, which is typical for a PIN diode. The p-type multiplication implant has a peak doping concentration of order 1×10^{16} cm^{-3} and has a significantly deeper profile into the bulk ($\approx 4\,\mu$m) than the n$^+$ electrode. The bulk material is high resistivity p-type silicon (approximately 10 kOhm-cm) with a p$^+$ anode electrode on the backside. An example of the doping concentration through the n-type cathode and p-type multiplication implant is shown in figure 2 (taken from [6]). To understand the high-field performance of the device the concept of the effective p-type doping areal density, Q$_{\text{effective}}$ is helpful, illustrated in figure 2 and defined as the net p-type doping concentration integrated over the depth of the implant. As a high resistivity p-type bulk is used a shallow uniform p-spray doping (order 1×10^{15} cm^{-3} and 4 μm deep) is implemented to isolate the cathodes. To reduce the magnitude of the electric field at the perimeter of each cathode an additional deep n$^+$ doping region (known as the Junction Terminating Extension, JTE) is present, discussed in more detail later.

The LGAD device is operated with the bulk over depleted. Incident radiation produces electron-hole pairs in the detector with drift towards the cathode and anode respectively. The maximum electric field in the device is between the n$^+$ cathode and the p-type multiplication electrode and is proportional to the square root of the p-type doping density and proportional to the square root of the external bias voltage (for a bias voltage significantly higher than the built-in potential) for an abrupt
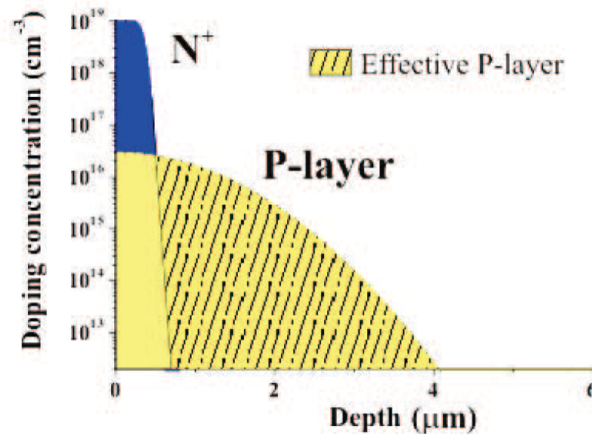
Figure 2. Example of doping profile throughout the N$^+$/P region (reproduced from [6] with permission).

junction approximation. Additional high-fields are present as the edge of the device and discussed later. The radiation induced electrons in the detector cross this high field region. For sufficiently high electric fields impact ionisation occurs which results in multiplication of the carriers and a signal gain. The electron-hole pair generation rate, G, due to impact ionisation is given by [7]

$$G = \alpha_n n v_n + \alpha_p p v_p \qquad (2.1)$$

where (n, p), (v_n, v_p) and (α_n, α_p) are the electron and hole density, velocity, and ionisation rate respectively. The ionisation rate strongly depends on the electric field (E) and maybe defined as

$$\alpha = \frac{E}{E_{th}} \exp[-E_i/E] \qquad (2.2)$$

where E is the high-field in the device, E_{th} is the high-field effective ionisation threshold energy (for silicon equal to 3.6 eV for electrons and 5.0 eV for holes) and E_i is the threshold field due to ionisation scattering. Increasing the high-field (either due to an increase in the doping density or an increase in the external bias voltage) will increase the electron-hole pair generation rate. For a low gain device, the desire is to have an overall gain of 10 at 200 V bias, with a breakdown voltage significantly higher than this at least 400 V. Simulation is presented which calculates the required doping profile to obtain such a gain and addresses issues related to low breakdown voltages.

3 LGAD simulation

The device simulation has been performed using Synopsis Sentaurus TCAD (Version G – 2012.06) [11] to understand the gain as a function of doping and the high voltage breakdown characteristics. Sentaurus Process was used to create the doping profiles using a simulated fabrication process based on a standard Micron Semiconductor PIN diode process modified with the additional p-type multiplication dopant. Sentaurus Device simulation was used to evaluate the electrical characteristics of the device, transient simulations using the heavy ion command for charge generation was used to simulate the device response to radiation. Radiation induced charge carriers were simulated by creating 80 electron-holes pairs deposited 5 µm from the backside p-type anode.

The collected charge was calculated by integrating the simulated current pulse. The gain of the LGAD device was calculated by comparing the collected charge to that simulated for a standard PIN diode. Simulations were performed initially on 1D structures to understand the device performance followed by 2D simulations to study high electric fields at the edge of the implants.

To correctly model the high-field effects the simulations were performed using the Okuto model [13] for impact ionisation. The Schenk model [14] was chosen to simulate band-to-band tunnelling, which is essential when dealing with high electric fields, as this best described the conditions under test. Importantly the model works up to an electric field of $\approx 8 \times 10^5$ V/cm and for doping levels at the anode and cathode greater than 1×10^{19} cm^{-3}.

The initial simulation produced the electric field profile through the LGAD device, shown in figure 3 for a reverse bias of 700 V. The p-type multiplication layer becomes fully depleted at a very low reverse bias of approximately 25 V after which the bulk depletes. The maximum electric field is, as required, at the interface of the n$^+$ cathode and the p-type multiplication implant. For significant impact ionisation to occur an electric field of $\approx 10^5$ V/cm (E_{crit}) is required. The E_{crit} is directly related to the doping concentration within the detector. The peak concentration in the lower doped side of the n$^+$p junction is in the range of 1×10^{16} cm^{-3}. According to Baliga [9] for a doping concentration in this range the E_{crit} value is in the range of 4×10^5 V/cm, however lower E-fields will still result in some gain.
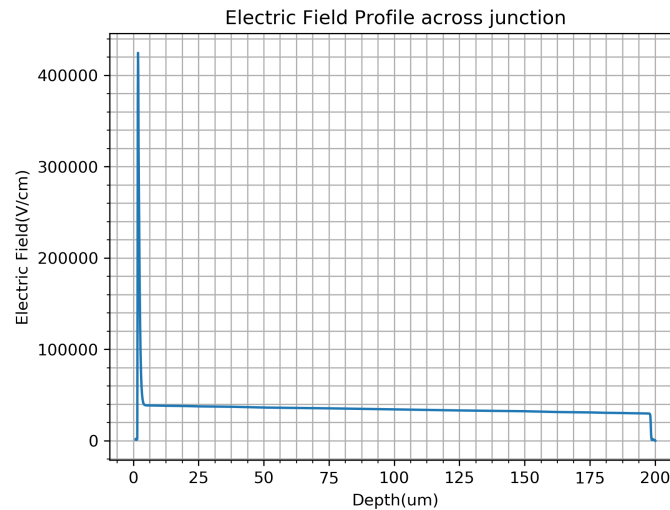

Figure 3. Typical electric field profile through device showing high electric field at junction between n+/p region. The device is 200 μm thick with a reverse bias of 700 V.

To investigate the effect of the p-type multiplication implant dose and doping profile on the device gain a series of simulations were performed for a range of boron implant dose concentrations and energies, while the phosphorus implant parameters were kept constant. A change in the p-type multiplication dopant level and distribution changes the $Q_{effective}$ of the device. The simulations demonstrated that the gain of the device is a function of $Q_{effective}$, shown in figure 4, for the LGAD under a reverse bias of 400 V. There is a strong correlation between gain and $Q_{effective}$ and a critical value of $Q_{effective}$, defined as $Q_{effective}^{crit}$, for which a gain of 1.1 is achieved, where $Q_{effective}^{crit} = 1.6 \times 10^{12}$ cm^{-2}. As the gain increases with increasing $Q_{effective}$ the breakdown voltage decreases

due to higher fields in the device at lower bias voltages. In this case the breakdown voltage is caused by the high electric field in the multiplication region between the n^+ implant and the p-type multiplication implant, as there are no edge effects present in the 1D simulated case. This simulation work agrees with the results shown in [6].

2D simulations were performed to investigate the breakdown voltage of the device due to field distribution at the edge of the LGAD implants. At the edge of the LGAD device the p-type multiplication implant can either align with the edge of the n^+ cathode or be smaller. Reduced multiplication implant size reduces the active fraction of the device and leads to a spatial variation in the response of the device and as such should be minimised. The edge region of the device shown in figure 1 was simulated using the process device simulation. The boundary conditions were reflective and only the last $30\,\mu m$ of the n^+ cathode implant was simulated. The simulated p-type multiplication implant region was $20\,\mu m$ wide, finishing $10\,\mu m$ before the n^+ cathode. The JTE implant extended $10\,\mu m$ from the edge of the multiplication implant. The p-spray implant was uniform over the full surface and the simulation extended $40\,\mu m$ from the end of the n^+ implant. The final dopant distributions extend beyond the implant regions due to dopant diffusion by up to $10\,\mu m$.

The maximum electric field on the cathode side of the device as a function of distance from the simulation boundary for the edge pixel in the array is shown in figure 5 for an applied bias of $200\,V$. The electric field is approximately constant at the interface between the n^+ cathode and the p-type multiplication implant (0 to $20\,\mu m$ in figure 5). The maximum electric field falls after the p-type implant ends and rises again towards the edge of the n^+ implant, at the interface of the n^+ cathode and the p-spray. Ideally, the maximum electric field should be in the multiplication junction so that premature breakdown is avoided. Without the JTE the electric field at edge of the n^+ cathode is larger than the electric field in the multiplication region and will result in breakdown taking place at this location. To reduce the field in the edge region a deep extension to the n^+ cathode was designed, known as the junction termination electrode JTE. The JTE is fabricated with the same doping concentration as the n^+ cathode implant, however it has a much longer diffusion time to obtain deeper dopant diffusion into the silicon. To reduce the edge electric field the JTE must be deeper than the p-type multiplication junction and wide enough to produce a gradual reduction in the potential to the p-spray implant. figure 5 shows the maximum electric field in the LGAD in the presence of a JTE. The maximum field in the edge region is reduced by a factor of two, for this design, and critically is less than the maximum field in the multiplication region.

The simulated high-voltage current-voltage characteristics of the device improves with the use of the JTE due to the lower maximum electric field in the edge region as shown in figure 5. The breakdown voltage of the device increases from $290\,V$ without a JTE to $780\,V$ with the JTE. The exact high voltage behaviour of the device depends on the details of the JTE doping density, diffusion depth and width. Devices manufactured with and without the JTE are discussed in the results section.

4 Devices

Using the information obtained from simulations as input to the fabrication process, LGAD devices were fabricated at Micron Semiconductor Ltd. They were characterised at the University of Glasgow in order to evaluate their electrical capabilities and gain performance. In total there were
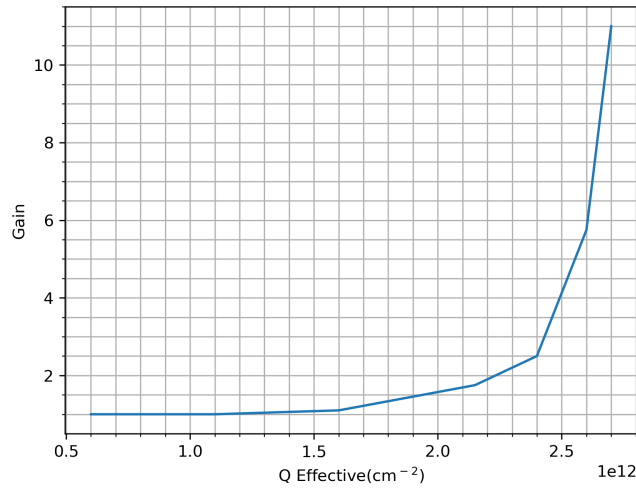
Figure 4. Simulated Gain against Q effective for a bias voltage of 400 V.
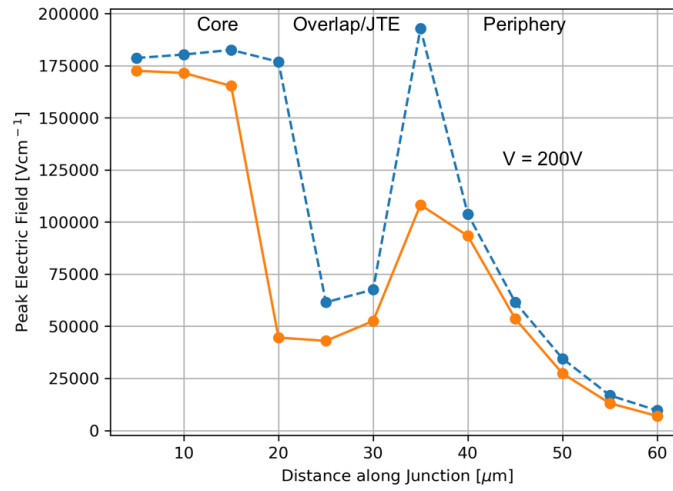

Figure 5. Simulated maximum electric field in the device for a bias of 200 V as a function of distance along the surface in the edge region of the n$^+$ junction for a device with and without a JTE. The caption is; simulated without JTE: dashed line, simulated with JTE: solid line.

104 devices fabricated each with an active area of 5×5 mm and varying periphery designs. The mask set included six different LGAD detector designs and six control designs. The six LGAD detector designs all had a JTE implant, but the p-type multiplication size varied relative to the n$^+$ junction. There were three sizes of the p-type layer, which were all smaller than the n$^+$ junction. For each size of the p-type layer there were two different overlapping metal designs, which acted as a field plate to further reduce high electric fields at the edge of the pixel implant. The control devices consisted of three designs again each design had two overlapping metal designs. The first control had no JTE implant, the second had no multiplication implant with a JTE and the third had neither a JTE implant or a multiplication implant. The wafer was p-type silicon with a resistivity of 8.5 kΩcm and a thickness of 300 μm.
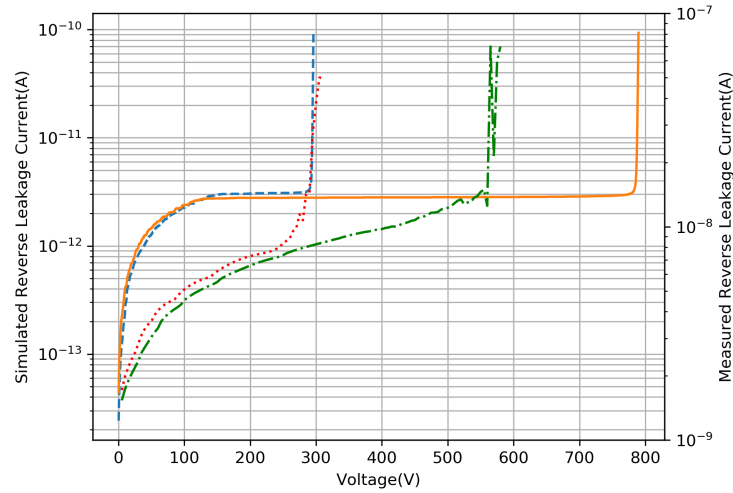
Figure 6. IV curves for simulated and measured LGAD devices with and without a JTE. The caption is; simulated without JTE: dashed line, simulated with JTE: solid line, measured without JTE: dotted line, and measured with JTE: dot-dashed line.

Based on the results from simulation several process runs were performed for a small range in boron implant energies and doses and for several JTE doses and drive-in times. The objective was to obtain the desired $Q_{effective}$, and therefore gain, and to increase the breakdown voltage as much as possible. To verify the doping profiles obtained from the TCAD simulations Secondary Ion Mass Spectroscopy (SIMS) was performed on devices from each wafer run for both the phosphorus and boron implants. Results from one run are shown in figures 7a and 7b respectively. The SIMS measurements match well with the TCAD doping profiles allowing us to be confident in both our fabrication process and our simulations. The simulation was tuned to the exact details of the fabrication process. Small changes in the fabrication process can make a significant change to the doping profiles and thus the $Q_{effective}$, resulting in changes to the device gain and breakdown voltage. This includes changes to the boron implant energy and dose, as well as changes to the implantation process. This was demonstrated in the simulations and shown to be the case in the fabricated devices.

5 Device characterisation

All devices have undergone IV characterisation in order to determine suitable devices for Transient Current Technique (TCT) measurements used to measured the gain. The IV measurements were performed on a probe station, where the reverse bias voltage was increased in 5 V steps from 0 to 1000 V, and the compliance current was set to 500 nA. The current characteristics varied across the wafer depending on the periphery design as described below. The devices had a leakage current between 40 and 100 nAcm^{-2} measured at 20°C and at 200 V.

Figure 6 shows the current-voltage curves for LGAD fabricated with and without a JTE, clearly showing the increased breakdown voltage capabilities with the JTE. The measured breakdown voltage of an LGAD with a JTE is > 500 V compared with that of an LGAD without a JTE of < 300 V. The fabricated results show reasonable agreement with simulation for the breakdown voltage. The measured devices with the JTE also show a lower plateau current due to the reduced
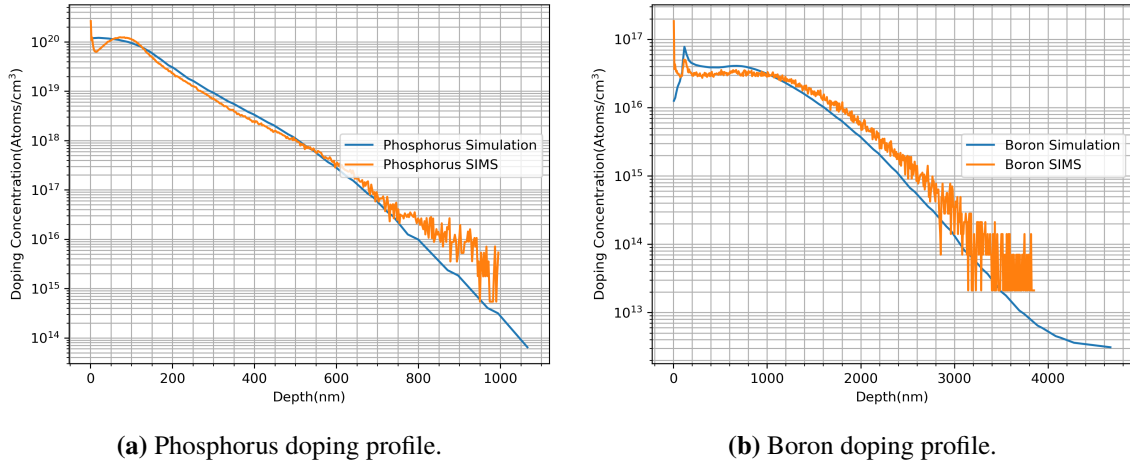
(a) Phosphorus doping profile.

(b) Boron doping profile.

Figure 7. Comparison of dopant profiles from simulation and SIMS measurements.

high fields at the edge of the device for a given bias voltage. The magnitude of the current values for the simulated and measured devices should not be compared as the simulated devices are dominated by the edge region because the p-type multiplication region is only $20\,\mu m$ wide compared to 5 mm for the real device.

TCT measurements were performed using the set-up produced by Particulars [12] using a 660 nm red laser focused to a spot with FWHM on $3\,\mu m$ on the centre of the backside of the device. The LGAD devices have a $500\,\mu m$ circular opening in centre of the back-side aluminium to allow light injection. A red laser has a penetration depth of $\approx 4\mu m$ in silicon, which is similar to that of a low energy x-ray. As the red laser is injected into the backside of the detector the electrons produced, due to ionisation, drift the width of the detector and undergo multiplication in the high field region producing internal gain. The output from the detector is amplified with a high-bandpass amplifier from Particulars (AM-01 A) and digitised with an oscilloscope (Agilent MSO9404A). The collected charge is measured by integrating the waveform in a 60 ns window centred on the waveform. The waveform also allows the rise time of the signal to be measured.

Illuminating from the backside with the red laser allows the determination of the full depletion voltage of the device. This was achieved by increasing the bias voltage in steps of 5 V and calculating the charge collected for each voltage in the range 0 to 200 V. The charge collected was plotted against bias voltage from which the full depletion voltage can be obtained as the point at which the two linear fits shown in figure 8 intersect. This is the point at which all charge deposited in the backside of the device is collected at the n⁺ junction. This was found to be 116 V which agrees with simulated results for the wafer resistivity. This is slightly higher than that of PIN diode as the multiplication region has to fully deplete (which requires ≈ 25 V) before depletion of the silicon bulk occurs.

Gain measurements were made for the device by measuring the collected charge for bias voltages above full depletion voltage in ten volt steps up to device breakdown. The charge collection measurements were obtained for both LGAD and over depleted PIN devices with the gain defined at the ratio of the two. It is important to study the laser output as a function of time as any change in the laser could alter the gain obtained significantly. Ideally we would like to have had a beam monitor set-up for this, however we do not. Instead we were able to manipulate the size of the
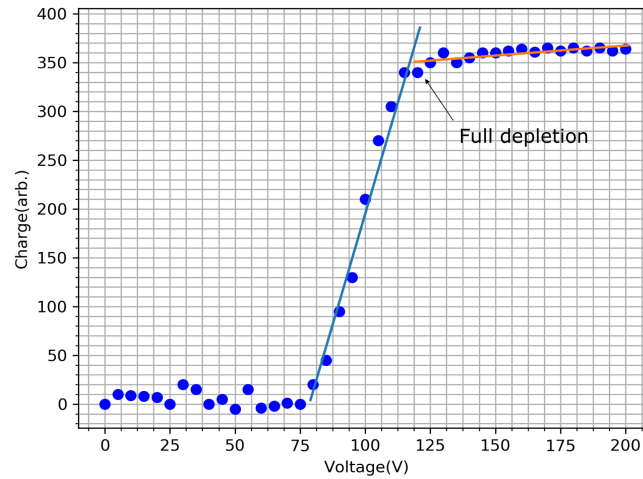
Figure 8. A TCT method for finding full the depletion voltage. Where the two fits intersect all charge deposited is collected and hence full depletion.

PIN diode curve to exactly match that of the first part of the LGAD waveform. Figure 9 shows a waveform comparison of a PIN diode and an LGAD device from backside red laser TCT in orange and blue respectively at 300 V. The shape of the signals differ significantly due to the avalanche process in the LGAD devices. The first part of the waveform is identical as the drift of electrons is controlled by the bulk electric field in the device, which is the same for both LGAD and PIN diodes. The curves differ after the kink in the LGAD waveform. This occurs at the onset of multiplication of electrons as can be seen on figure 9. The pulse also shows where there is a drift of holes to the backside after incoming electrons have produced e-h pairs under impact ionisation.
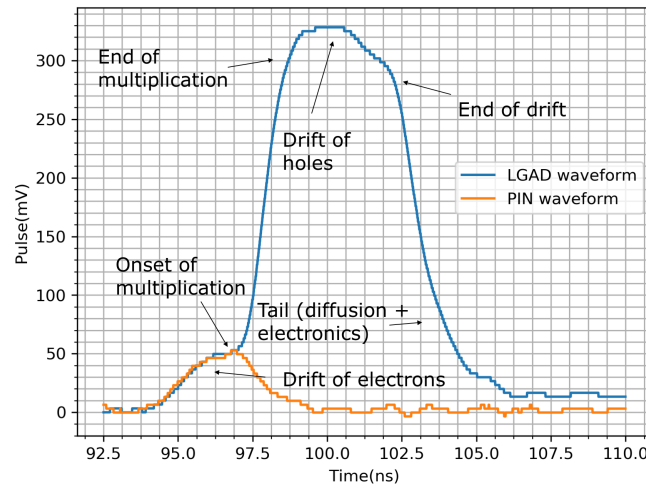

Figure 9. Comparison of waveforms produced by red laser backside TCT for both LGAD and PIN diodes in blue and orange respectively at 300 V.
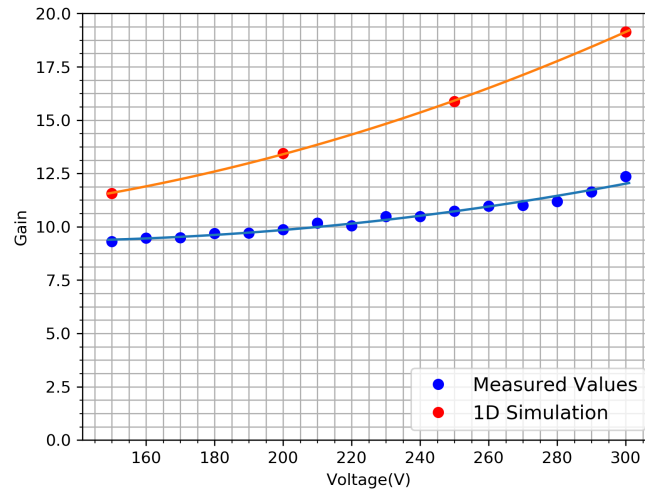
Figure 10. Measured gain as a function of voltage in gain range of 9–12.
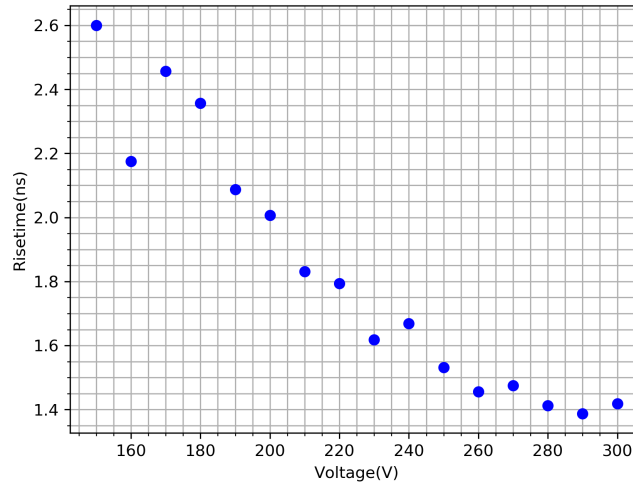

Figure 11. Measured rise time as a function of voltage.

The measured gain as a function of bias voltage is shown in figure 10. The gain increases from 9 to 12 for the applied bias voltage range of 150 to 300 V. The measured gain is compared to the simulated gain for a 1D device. The two sets of data are in broad agreement but do not match perfectly with the measured values being lower than simulation (measured gain is 10 and simulated is 13.5 at 200 V bias) and showing a slower rise in gain as a function of bias voltage. Both effects are consistent with a lower $Q_{effective}$ in the fabricated device than the simulated device. It has been shown that the gain of the device is very dependant on the $Q_{effective}$. A small change in this value can have a large impact on the gain achieved as shown in figure 4. Many fabrication factors can contribute to small changes in the doping profile as fine control of the implant dose, the doping concentration and profile can be difficult. This is due to several fabrication processes, including; control and calibration of the ion implanter, presence and thickness of oxide over the silicon during implantation and the exact thermal history of the device during the various fabrication steps. It

is shown in figures 7b and 7a that the simulated doping profiles don't match exactly that of the fabricated devices especially near the surface of the device, which is one reason why the measured gain values differ from simulation. Additionally, within the simulation software it is possible to introduce some random variation in the doping profile, controlled by a random seed generator in the numerical calculation, which is seen most drastically in the phosphorus doping profile. This produces some statistical uncertainty in simulated value, however this information is not included in figure 10. For the low energy x-ray detection a gain of ten is required and this has been achieved with these devices.

The rise time of the signal is calculated as the time between 20% and 90% of the pulse height. Figure 11 shows the rise time as a function of voltage for the device reported in figure 10. The rise time falls with increasing bias voltage and has a value of 1.4 ns at 300 V. Thinner devices will increase the rise time as the drift distances are reduced.

6 Conclusion

Low Gain Avalanche Detectors have been simulated and then fabricated at Micron Semiconductor Ltd with a process based on the simulation results.

The simulation shows that the gain is strongly dependent upon the effective p-type doping areal density, $Q_{effective}$, defined as the net p-type doping concentration integrated over the depth of the implant. For a $Q_{effective}$ above a critical value ($Q_{effective}^{crit}$) of 1.6×10^{12} cm^{-2} the gain increases steeply with doping concentration. The breakdown voltage of the device has been shown to be strongly affected by the electric field at the edge of the n$^+$ cathode. Simulation shows significant improvements in breakdown performance with a JTE structure, with the breakdown voltage increasing from 290 V without a JTE to 780 V with the JTE.

Detailed understanding of the device fabrication process allowed simulation to obtain reasonable agreement with real doping profiles obtained from SIMS. However, small changes in the simulation give rise to changes in the doping profiles, which change the gain of the device in the range of 10%.

LGAD diode detectors have been fabricated and show excellent electrical properties of low leakage current and reasonably high breakdown levels and a gain of 10.

The fabricated LGAD detectors demonstrate the expected increase in breakdown voltage with the inclusion of a JTE. Measured values increased from < 300 V without a JTE to > 500 V with a JTE. The measured current in the device was between 40 and 100 nAcm^{-2} measured at 20°C and at 200 V

The measured gain of the LGAD was ten at 210 V, measured for 660 nm light illumination. The gain showed a dependence with voltage and increased to 12.5 at 300 V.

The results shown in this paper show that LGAD detectors fabricated at Micron Semiconductor Ltd can produce the required gain for both particle physics and x-ray applications. Further process developments are underway to improve the yield and reproducibility of these results. The near future plans are to make x-ray fluorescence measurements at the University of Glasgow and the design of a new mask set to include pad diodes, strip detectors and Medipix pixel arrays. We aim to include a shallow backside P$^+$ in order to detect low energy x-rays which inherently have a shallow penetration depth in silicon.

Acknowledgments

References

[1] G. Lutz, *Semiconductor radiation detectors*, Device Physics, Springer, (2007).

[2] T. Hatsui and H. Graafsma, *X-ray imaging detectors for synchrotron and XFEL sources*, *IUCrJ* **2** (2015) 371.

[3] D. Renker, *New trends on photodetectors*, *Nucl. Instrum. Meth.* **A 571** (2007) 1.

[4] P.P Webb and A.R. Jones, *Large area reach-Through Avalanche Diodes for radiation monitoring*, *IEEE Trans. Nucl. Sci.* **21** (1974) 151.

[5] X. Llopart, R. Ballabriga, M. Campbell, L. Tlustos and W. Wong, *Timepix, a 65k programmable pixel readout chip for arrival time, energy and/or photon counting measurements*, *Nucl. Instrum. Meth.* **A 581** (2007) 485 [*Erratum ibid.* **A 585** (2008) 106].

[6] I. Cortés, P. Fernández-Martínez, D. Flores, S. Hidalgo and J. Rebollo, *Gain estimation of RT-APD devices by means of TCAD numerical simulations*, proceedings of the *8th Spanish Conference on Electron Devices CDE 2011*, Palma de Mallorca, Spain, 8–11 February 2011.

[7] S.M. Sze, *Physics of Semiconductor Devices*, second edition, Wiley, New York U.S.A., (1969), ISBN-471-84290-7.

[8] G. Pellegrini et al., *Technology developments and first measurements of Low Gain Avalanche Detectors (LGAD) for high energy physics applications*, *Nucl. Instrum. Meth.* **A 765** (2014) 12.

[9] B. Jayant Baliga, *Fundamentals of Power Semiconductor Devices*, Springer Science, (2008).

[10] P. Fernández-Martínez et al., *Design and Fabrication of an Optimum Peripheral Region for Low Gain Avalanche Detectors*, *Nucl. Instrum. Meth.* **A 821** (2016) 93 [`arXiv:1510.08626`].

[11] *Sentaurus user Guide*, Synopsys, (2010).

[12] Particulars advanced measurement systems, http://Particulars.si.

[13] Y. Okuto and C.R. Crowell, *Threshold Energy Effect on Avalanche Breakdown Voltage in Semiconductor Junctions*, *Solid State Electron.* **18** (1975) 161.

[14] A. Schenk, *Rigorous Theory and Simplified Model of the Band-to-Band Tunneling in Silicon*, *Solid State Electron.* **36** (1993) 19.